

# Emulsion Formation in Dripping Regime of Co-Flowing Immiscible Liquids in Co-Axial Micro-Tubes

In-Hwan Yang and Mohamed S. El-Genk\*

Institute for Space & Nuclear Power Studies and Chemical & Nuclear Engineering Dept.  
University of New Mexico, Albuquerque, NM, USA

## ABSTRACT

Numerical analysis is performed of the formation of an emulsion of disperse micro-drops in the dripping regime of co-flowing immiscible liquids in co-axial micro-tubes. This parametric analysis investigated the effects of changing the interfacial tension, velocities and viscosities of the two liquids and the diameters of the coaxial micro-tubes on the dynamics, frequency and radius of the forming droplets. The transient, 2-D axisymmetric Navier-Stokes equations of the two liquids and the advection equation for the interface, subject to the momentum jump condition, are solved using a finite element method. Semi-empirical correlations are developed for the dimensionless radius and formation frequency of the droplets, based on numerical results for wide ranges of parameters. The correlations are in good agreement (+10% to -14%) with recently reported experimental measurements for water (mono-disperse) droplets in a continuous flowing salad oil in a co-axial micro-tube.

## NOMENCLATURE

$Ca_c$	Capillary number of continuous flow, $\mu_c \bar{u}_c / \sigma_{d,c}$
$Ca_d$	Capillary number of disperse flow, $\mu_d \bar{u}_d / \sigma_{d,c}$
$f$	Frequency of forming droplets (Hz)
$f^*$	Dimensionless frequency, $f_{mb} R_d / u_d$
$g$	Acceleration of gravity ( $m/s^2$ )
$g^*$	Dimensionless gravity, $g(\rho_d R_d^2 / (\bar{u}_d \mu_d))$
$L$	Length of micro-tube ( $\mu m$ )
$P$	Pressure, Pa
$P^*$	Dimensionless pressure, $p R_d / (\bar{u}_d \mu_d)$
$Q$	Liquid flow rate ( $\mu l/s$ )
$R$	Microtube radius ( $\mu m$ )
$R^*$	Ratio of microtubes radii, $R_c / R_d$
$u$	Flow velocity, m/s
$\bar{u}_d$	Injection velocity of disperse liquid, $Q_d / (\pi R_d^2)$ (m/s)
$\bar{u}_c$	Injection velocity of continuous liquid, $Q_c / (\pi(R_c - R_{d,o})^2)$ (m/s)
$u^*$	Dimensionless velocity, $\vec{u} / \bar{u}_d$
$r$	Radial distance ( $\mu m$ )
$r_d^*$	Dimensionless radius of disperse droplet, $r_d / R_d$
$Re_d$	Reynolds number of dispersed liquid, $2R_d \rho_d \bar{u}_d / \mu_d$

\*Corresponding author. Regents' Professor and Director, Tel: (505) 277 - 5442, E-mail: mgenk@unm.edu

$Re_c$	Reynolds number of continuous liquid, $2(R_c - R_{d,o}) \rho_c \bar{u}_c / \mu_c$
$t$	Time (s)
$t^*$	Dimensionless time, $t \bar{u}_d / R_d$
$z$	Axial distance ( $\mu\text{m}$ )
$z^*$	Dimensionless axial distance, $z / R_d$
$We_d$	Weber number of disperse liquid, $2R_d \rho_d \bar{u}_d^2 / \sigma_{d,c}$

**Greeks**

$\varepsilon$	Thickness of interfacial layer ( $\mu\text{m}$ )
$\phi$	Distance function of interface ( $\mu\text{m}$ )
$\phi^*$	Normalized shape function, $\phi / R_d$
$\gamma$	Reinitialization parameter ( $\mu\text{m/s}$ )
$\kappa$	Interface curvature ( $\text{m}^{-1}$ )
$\kappa^*$	Dimensionless interface curvature, $\kappa R_d$
$\mu$	Liquid viscosity (Pa·s)
$\mu^*$	Dimensionless viscosity, $\mu / \mu_d$
$\mu_r$	Viscosity ratio, $\mu_d / \mu_c$
$\rho$	Liquid density ( $\text{kg/m}^3$ )
$\rho^*$	Dimensionless density, $\rho / \rho_d$
$\rho_r$	Density ratio, $\rho_d / \rho_c$
$\sigma_{d,c}$	Interfacial tension (N/m)

**Subscripts**

$c$	Continuous
$d$	Disperse
$int$	Interface
$mb$	Mass balance
$num$	Numerical
$o$	outer
$ref$	Reference

**1. INTRODUCTION**

Emulsions of mono-disperse micro-drops have been the subject of extensive investigations. The aim is to generate mono-disperse droplets of controllable sizes, ranging from a fraction to 10's of microns, at high frequencies. An emulsion is a mixture of two immiscible liquids in which one liquid in the form of droplets is dispersed in a continuous phase of the second liquid. Emulsions are encountered in chemical; petroleum; energy; pharmaceutical; food processing and cosmetics industries and used in medical procedures; drug delivery; polymerization processing; microanalysis; extraction processes and microsystems [1–7].

Conventional methods to produce emulsions involve injecting a liquid at a constant flow rate through an orifice or a capillary tube [8, 9] into a continuous immiscible liquid that is quiescent or dynamically inactive. These methods are inefficient because the bulk of the dispersed liquid is not used. In addition, the production rates of disperse droplets are relatively low and the emulsions are highly poly-disperse. To overcome some or all these limitations, recent techniques of membrane extrusion, micro-thread generation and viscoelastic shear have been proposed [6, 10, 11]. Although more effective, each technique has some inherent limitations. For example, the poly-dispersity in the emulsion produced using membrane emulsification is ~10% of the average drop size [6], and as much as 16% in production condition using the viscoelastic shear technique [10]. A good control of the size,

production frequency and the dynamics of forming disperse droplets, is achieved using co-flowing immiscible liquids. This method not only provides better control of the droplet volume, but also produces highly mono-disperse emulsions [4, 5, 12].

The production of micro-emulsions in a gravitation field is the focus of this paper. The term micro-emulsion is used in reference to producing mono-disperse droplets with diameters ranging from a few to 10's of microns. The forming droplets of disperse liquid at the tip of the inner micro-tube, grow, deform and eventually detach, or pinch off in a cyclical fashion. The formation dynamics of the droplets and the effects of the various controlling parameters have been investigated experimentally [1, 4, 5, 12–18] and numerically [18–24].

In emulsions produced using co-flowing immiscible liquids in co-axial micro-tubes, two mechanisms of forming disperse droplets have been observed experimentally [15, 16] and predicted numerically [20–24]. These are: (a) *dripping*, in which the forming droplet detaches directing off the tip of the inner micro-tube, and (b) *jetting*, in which the forming droplet detaches at the end of an extended thread or filament of the disperse liquid, some distance downstream from the tip of the inner micro-tube. The highly mono-disperse emulsion produced by the first mechanism prevails at low flow rates of disperse and continuous liquids. By contrast, the forming emulsions in the jetting regime at high liquids flow rates could be highly poly-disperse. For both mechanisms, increasing the flow rate of the continuous liquid decreases the size and increases the forming frequency of the droplets. In these mechanisms, there is a great degree of control on the operating parameters for producing the droplets, owing to the large interfacial area between the two, co-flowing immiscible liquids. The formation of mono-disperse droplets in the dripping regime evolves in three successive stages: (a) steady growth; (2) deformation and necking; and (3) detaching or pinch off (Fig. 1a–1c).

Umbanhowar et al. [4] have shown experimentally that an emulsion with a poly-dispersity of  $< 3\%$  can be produced using co-flowing immiscible liquids. On the other hand, Anna et al. [12] have shown that, depending on the flow rates of the co-flowing liquids, both mono-disperse and poly-disperse droplets could be generated. These and other recent investigations have shown that the continuous liquid flow focuses the flow of the disperse liquid. This reduces the volume and increases the formation frequency of disperse droplets and promotes mono-dispersity; a desirable property in various applications of micro-emulsions.

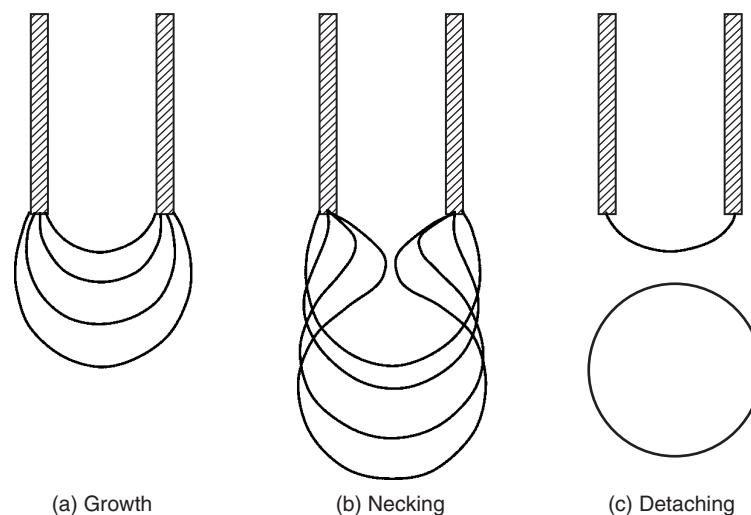


Figure 1. Growth, necking and detaching (or pinch-off) of a disperse droplet at the tip of a micro-tube in a continuous co-axial flow of an immiscible liquid.

The formation dynamics of disperse droplets in a system of two co-flowing immiscible liquids depend on many parameters, which are easily controlled in an experiment or industrial production. These are the average flow rates (or injection velocities), dynamic viscosities and densities of the continuous and disperse liquids; the diameters of the co-axial micro-tubes and the interfacial tension. The reported experimental results for emulsions using co-flowing immiscible liquids have contributed greatly to the understanding of the effects of the different parameters on the droplet formation in the dripping and jetting regimes. Experiments, however, have inherent limitations because of using intrusive measurement techniques and the imprecise measurements of droplets diameters less than  $80\ \mu\text{m}$  [13]. Instead, numerical simulation can be used to gain an understanding of the prevailing processes and quantify the effects of the different parameters. Numerical simulations, though not a substitute for experimental investigations, are relatively less expensive and time consuming. They could be useful for gaining more insight into the formation dynamics of the disperse droplets and characterizing the flow fields of the continuous liquid and within the disperse droplets, thus complementing the experimental findings and helping in the interpretation of results. There is not a credible substitute to using experimental data for validating the simulation methodologies and the fidelity of the numerical results.

Numerical simulations of the formation of disperse droplets in a system of co-flowing immiscible liquids in coaxial micro-tubes have used different methods to solve the transient Navier-Stokes equations of the liquids, subject to the momentum jump condition at the interface. These simulations track the growth, surface topology, necking and the eventual pinch off of the disperse droplets. Numerical methods used include the boundary element method (BEM) [23], and the volume-of-fluid (VOF) [20, 25], the continuum surface force (CSF) [26], and the front tracking methods [22]. In addition, commercial software packages such as FLUENT [21, 27] and COMSOL Multiphysics [18] have been used to investigate the same system.

Zhang [24] and Zhang and Basaran [9] have studied, both experimentally and numerically, the dynamics of forming disperse droplets in a quiescent and a continuous co-flowing immiscible liquid. Hong and Wang [21] numerically investigated the effect of the ratio of the injection rates of the co-axial, co-flowing liquids on the size of the forming droplets. Their results suggested that when the ratio of the injection rate of the disperse liquid to that of the continuous liquid is  $< 0.1$ , the flow rate of the disperse liquid barely affects the size (or the diameter) of the forming droplets. The effects of the continuous and disperse liquids flow rates and viscosities and the interfacial surface tension on the formation dynamics of disperse droplets have been investigated numerically by Hua et al. [22].

In summary, the reported experimental and numerical simulation results have enhanced the understanding of the regimes and dynamics of forming disperse droplets using co-flowing immiscible liquids in co-axial micro-tubes. Despite the extensive experimental and numerical work reported, additional work is needed to develop predictive correlations for the radius and formation frequency of the disperse droplets in terms of the prevailing operating parameters.

Such predictive correlations would be useful for industrial production, prototype designs and estimating the radius and forming frequency of disperse droplets. Experimental measurements of the effects of various controlling parameters on the radius and forming frequency of disperse droplets in the dripping regime is quite limited to develop suitable correlations. Thus, the motivation for the present work is to develop, based on the results of numerical simulations covering wide ranges of controlling parameters, predictive semi-empirical correlations for the radius and formation frequency of disperse droplets in the dripping regime.

In the dripping regime, which is the primary focus of this paper, the drag force exerted by the continuous liquid flow onto the interface with the growing disperse droplet causes necking and eventual pinch off of the droplet. In this regime, a precise control of the size and frequency of the forming droplets is possible by varying the flow rates of the co-flowing liquids. Forming either mono-disperse or poly-disperse droplets in the dripping regime depends on the flow rates and properties of the continuous and disperse liquids, the diameters of the co-axial micro-tubes, and the interfacial surface tension.

This paper presents the results of numerical simulations on forming micro-droplets of a disperse liquid in a continuous immiscible liquid, co-flowing in a co-axial micro-tube. These simulations investigate the contributions of various parameters affecting the formation dynamics and frequency and the radius of disperse droplets. The simulations solve the transient, 2-D axisymmetric Navier-Stokes equations in the computational domains of the co-flowing liquids and the advection equation of the interface between the two immiscible liquids, subject to the prevailing momentum jump condition at the interface. The numerical solution of these equations uses a finite element method based on the capabilities of the commercial software COMSOL Multiphysics, version 4.0 [28].

The numerical simulations track: (a) the disperse droplet’s transient growth and eventual pinch off; (b) the evolving interface between the co-flowing liquids during the initial formation and growth of the disperse droplet, and (c) the induced liquid circulation inside the forming disperse droplet at different stages of growth to an eventual pinch off. The obtained numerical results of the effects of different controlling parameters are used to develop empirical correlations for the dimensional radius and formation frequency of the disperse droplets in terms of the capillary number of the continuous liquid and the ratios of Reynolds numbers and diameters of micro-tubes of the co-flowing immiscible liquids. To validate the numerical results and the developed correlations, values of the disperse droplet radius are compared to those obtained numerically by Hua et al. [22] and to recently reported experimental measurements by other investigators [17] for water-salad oil flows in co-axial micro-tubes.

**2. PROBLEM STATEMENT**

Numerical analysis is performed to simulate the formation of a disperse droplet of an incompressible and Newtonian liquid at the tip of a micro-tube with an inner radius,  $R_d$ , in a co-flowing immiscible, incompressible and Newtonian liquid in a concentric micro-tube of a larger radius  $R_c$  ( $R_c > R_d$ ) (Fig. 2). The disperse liquid has a dynamic viscosity,  $\mu_d$ , and a density,  $\rho_d$ , and the continuous liquid has a dynamic viscosity,  $\mu_c$ , and a density,  $\rho_c$ . The numerical analysis investigated the effects of the different parameters on the formation frequency and radius of the forming disperse droplets in the dripping regime. These parameters are the interfacial surface tension and the velocities, viscosities, and radii of the micro-tubes for the co-flowing immiscible liquids. The ranges of parameters investigated in the present numerical analysis are listed in Table 1.

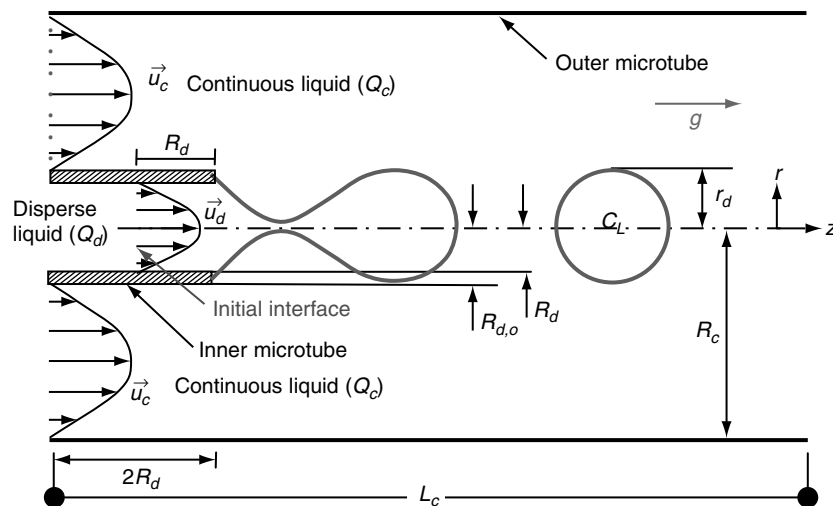


Figure 2. A schematic of a disperse droplet forming in a co-flowing immiscible liquid in a larger co-axial micro-tube.

Table 1. Ranges of properties and parameters investigated in numerical simulations.

Parameter	Value / Range	Units
Inner micro-tube radius, $R_d$	50–100	$\mu\text{m}$
Outer micro-tube radius, $R_c$	160–2020	$\mu\text{m}$
Disperse liquid viscosity, $\mu_d$	0.0078–0.124	$\text{Pa}\cdot\text{s}$
Continuous liquid viscosity, $\mu_c$	0.0078–0.124	$\text{Pa}\cdot\text{s}$
Disperse/continuous liquid density, $\rho_d / \rho_c$	1000 / 1000	$\text{kg}/\text{m}^3$
Interracial tension, $\sigma_{d,c}$	0.008–0.19	$\text{N}/\text{m}$
Disperse liquid rate/ velocity, $Q_d / \bar{u}_d$	0.22–0.97 / 0.007–0.031	$\mu\text{l}/\text{s}$ / $\text{m}/\text{s}$
Continuous liquid rate / velocity, $Q_c / \bar{u}_c$	0.16–9,900 / 0.0023–2.48	$\mu\text{l}/\text{s}$ / $\text{m}/\text{s}$
Micro-tubes radii ratio, $R^* (R_c / R_d)$	3.2–20.2	—
Disperse liquid Reynolds number, $Re_d$	0.045–0.8	—
Continuous liquid Reynolds number, $Re_c$	0.015–576	—
Continuous liquid Capillary number, $Ca_c$	0.001–0.55	—
Disperse liquid Capillary number, $Ca_d$	0.0023–0.08	—
Disperse liquid Weber number, $We_d$	0.0001–0.016	—
Reynolds numbers ratio ( $Re_d / Re_c$ )	0.0003–5.0	—

The disperse liquid injected at a constant volumetric flow rate,  $Q_d$ , emerges from the tip of the inner co-axial micro-tube into the continuous liquid injected also at a constant, but higher rate,  $Q_c$ , in the outer coaxial micro-tube (Fig. 2). Fully developed laminar velocity profiles are applied to the co-flowing liquids at the entrance of the coaxial micro-tubes. The length of computation domain ( $L_c = 30$  to  $60 R_d$ ) in the present numerical simulations is selected sufficiently long for simulating at least 3 cycles of forming the disperse droplet, including initial formation, growth and pinch off. The disperse droplet forming at the tip of the inner micro-tube grows steadily and develops a narrowing neck that eventually leads to a pinch off. This occurs when the net balance of the forces acting on the disperse droplet becomes positive (Fig. 1).

The gravitational force,  $g$ , in the computational domain (Fig. 2) is aligned with the centerline,  $C_L$ , of the co-axial micro-tubes. Owing to the low rates of the two immiscible liquids, the numerical simulations neglect viscous heat dissipation. They assume non-slip conditions at all liquid-solid interfaces (Fig. 2) and constant densities and viscosities of the co-flowing immiscible liquids. As listed in Table 1, the densities of both liquids are taken to be equal.

### 3. GOVERNING EQUATIONS AND SOLUTION METHODOLOGY

The present numerical simulations solve the transient momentum balance and continuity equations for the two co-flowing immiscible liquids, subject to the prevailing momentum jump condition at the surface of the evolving disperse droplet. The calculated results include: (a) the flow fields of the continuous liquid and inside the growing disperse droplet; (b) the local rate of momentum transfer and movement of the droplet surface as functions of the surface local curvature and (c) the droplet formation, growth and eventual pinch off. The momentum jump condition across the interface between the growing disperse droplet and the co-flowing continuous liquid is incorporated into the numerical solution using the Level set method [28–30]. The multiphase flow model in COMSOL Multiphysics commercial software, version 4.0a [28] uses this method for predicting the motion of the interface and the evolving shape of the disperse droplet during its growth to an eventual pinch off.

The momentum balance and continuity equations for the two co-flowing incompressible, Newtonian, and immiscible liquids in a gravitational field (Fig. 2) are given as:

(a) *Continuity Equations:*

$$\nabla \cdot \vec{u}_c = 0, \quad \text{and} \quad \nabla \cdot \vec{u}_d = 0. \quad (1)$$

**(b) Momentum Balance Equations:**

$$\begin{aligned}\rho_c \frac{\partial \vec{u}_c}{\partial t} + \rho_c \vec{u}_c \cdot \nabla \vec{u}_c &= -\nabla p + \mu_c \nabla^2 \vec{u}_c + \rho_c g + F \delta \\ \rho_d \frac{\partial \vec{u}_d}{\partial t} + \rho_d \vec{u}_d \cdot \nabla \vec{u}_d &= -\nabla p + \mu_d \nabla^2 \vec{u}_d + \rho_d g + F \delta\end{aligned}\quad (2)$$

In equation (3a),  $\tau_c$  and  $\tau_d$  are the shear stresses at the interface due the continuous and the disperse liquids flows, and  $\vec{n}$  is a normal vector to the interface. The delta function ( $\delta$ ) in equation (2) is unity at the interface and zero elsewhere in the computation domain. The interfacial force,  $F$ , in the momentum balance equations (2) is obtained from the application of the momentum jump condition at the interface. This condition, Equation (3a), equates the difference in hydrodynamic stresses exerted onto the interface by the co-flowing liquids to the normal stress associated with the local curvature of the interface and interfacial surface tension as:

$$\vec{n} \cdot [\tau_c - \tau_d] = F, \quad (3a)$$

Where,

$$F = \sigma_{d,c} \vec{n} (\nabla \cdot \vec{n}) = \sigma_{d,c} \vec{n} \kappa. \quad (3b)$$

In equation (3b),  $(\nabla \cdot \vec{n})$  is replaced by the curvature of interface,  $\kappa$ , based on the principal radii of curvature. The motion of the impermeable surface of the disperse droplet is described by the advection equation at the interface between the co-flowing immiscible liquids:

$$\frac{\partial \phi}{\partial t} + \vec{u}_{\text{int}} \cdot \nabla \phi = 0 \quad (4)$$

In this equation,  $\phi(r, z)$  is a scalar function that indicates the surface of the disperse droplet. The momentum balance and continuity equations are expressed in a dimensionless form as:

$$\nabla \cdot u^* = 0. \quad (5)$$

$$0.5 \rho^* \text{Re}_d \frac{\partial u^*}{\partial t^*} + \rho^* u^* \cdot \nabla u^* = -\nabla p^* + \mu^* \nabla^2 u^* + \rho^* g^* + \frac{1}{Ca_c \mu_r u_r} \vec{n} \kappa^* \delta. \quad (6)$$

These equations are solved numerically, subject to the condition of non-slip at the walls of the co-axial micro-tubes and assuming axisymmetric co-axial flows of the continuous and disperse immiscible liquids (Fig. 2). In addition, the isothermal co-axial liquid flows are assumed fully developed, with their average velocities determined from the volumetric flow rates at the inlet of the co-axial micro-tubes (Fig. 2). The length of the inner co-axial micro-tube is taken to be 2 times its inner radius ( $L_d = 2 R_d$ ) (Fig. 2).

At the start of the transient simulation,  $t = 0$ , the disperse liquid fills the inner micro-tube half way and the continuous liquid fills the rest of the computation domain. The initial flat interface between the two liquids is located a distance  $R_d$  from the tip of the inner micro-tube (Fig. 2). Equations (5) and (6) are solved simultaneously with the dimensionless form of equation (4), expressed as:

$$\frac{\partial \phi^*}{\partial t^*} + u_{\text{int}}^* \cdot \nabla \phi^* = 0. \quad (7)$$

The numerical solution of these coupled nonlinear Equations tracks the movement and the evolution of the surface and the growth of disperse droplet (Figs. 1a–1c).

#### 4. NUMERICAL SOLUTION METHODOLOGY AND VALIDATION

The Level set method for implementing the momentum jump condition in the numerical solution at the interface between the co-flowing immiscible liquids [28–30], uses the function  $\phi(r, z)$  to indicate the normal distance from the moving and evolving interface, or the surface of the disperse droplet, throughout the computation domain. In order to deal with the non-linearity of the momentum jump condition, (Eq. (3b)), without causing a numerical instability, a function  $H_\phi$  is introduced and assigned values of 1 and 0, for disperse and continuous liquid, respectively, thus:

$$\begin{cases} H_\phi = 1, & \text{if } \phi < 0 & \text{Disperse liquid} \\ H_\phi = 0.5, & \text{if } \phi = 0 & \text{Interface} \\ H_\phi = 0, & \text{if } \phi > 0 & \text{Continuous liquid} \end{cases} \quad (8)$$

Based on these notations, Eq. (7) can be rewritten in terms of the function,  $H_\phi$ , as;

$$\frac{\partial H_\phi}{\partial t^*} + u_{\text{int}}^* \cdot \nabla H_\phi = 0. \quad (9)$$

The solution of this equation gives the exact motion of the interface. However, in order to implement it numerically, while avoiding possible solution instability, Eq. (9) is expressed as:

$$\gamma \nabla \cdot (\varepsilon H_\phi - H_\phi(1 - H_\phi) \frac{\nabla H_\phi}{|\nabla H_\phi|}) = 0. \quad (10)$$

The value of the parameter,  $\gamma$ , indicates the desired level of stabilization or the amount of reinitialization for the level set method [28–30]. The appropriate value of the parameter,  $\gamma$ , which is a problem specific, ensures the stability of the numerical solution and the correct prediction of the movement of the interface.

The interface separating the growing disperse droplet from the continuous liquid flow is treated as a very thin layer,  $\varepsilon$ , with average liquid properties and a linear change in momentum across ( $H_\phi$  from 0 to 1). The liquid properties within the interface layer expressed in terms of those of the continuous and disperse liquids, are:

$$\begin{aligned} \rho &= \rho_c + (\rho_d - \rho_c) H_\phi \\ \mu &= \mu_c + (\mu_d - \mu_c) H_\phi \end{aligned} \quad (11)$$

Also, the unit normal vector to the interface,  $\vec{n}$  and the curvature of the interface,  $\kappa$ , are expressed as:

$$\vec{n} = \frac{\nabla H_\phi}{|\nabla H_\phi|}, \quad \kappa = \nabla \cdot \frac{\nabla H_\phi}{|\nabla H_\phi|} \quad (12)$$

The numerical solution of equation (10) uses an implicit method to ensure the stability of the simulation. The thickness of the interface layer,  $\varepsilon$ , is taken equal to the numerical mesh size ( $5 \mu\text{m}$ ) and the stability, or reinitialization parameter,  $\gamma$ , is taken as:

$$\gamma = \left( (Q_c + Q_d) / \pi R_c^2 \right). \quad (13)$$

In the present numerical simulations, the used mesh grid for the computation domain of the co-flowing immiscible liquids in the co-axial micro-tubes (Fig. 2) is comprised of quadrilateral elements of a uniform size ( $5 \mu\text{m} \times 5 \mu\text{m}$ ). The total number of the numerical mesh elements used, which increases commensurate with radius of the continuous liquid micro-tube, varied from 9,560 to 60,650. The selected length of the computation domain provide enough distance, from the tip of the disperse liquid inner micro-tube, to observe the formation and pinch-off of at least 3 disperse droplets, including the first one.

Using a finer grid, with a larger number of smaller quadrilateral elements, insignificantly changes the results of the simulation, including the diameter and the formation frequency of the disperse droplet, but markedly increases the computation time. With the size and the number of the numerical mesh elements used in the present simulations, the solution fully converges with  $< 6\%$  error in the mass balance of the disperse liquid for forming the droplets. The numerical simulations are performed using a cluster of 8 quad core processors (2.27 GHz Xeon) and 120 GB of memory. The real computation time for the simulations varied from 72 to 168 hours per case, depending on the size of the computation domain, radii of the co-axial micro-tubes and the selected properties of the disperse and the continuous liquids.

The results of the present numerical simulations are validated by comparing the obtained values of the disperse droplet radius with those reported by Hua et al. [22]; details are given next. Later in the results section, the developed semi-empirical correlation for the dimensionless radius of the disperse droplet, based on the results of the present numerical simulations, is compared with recently reported experimental measurements in the dripping regime of co-flowing water (disperse) and salad oil (continuous) in co-axial micro-tubes [17].

#### 4.1. Validation of numerical simulation results

To validate the results of the present numerical simulations, the calculated values of the radius of forming disperse droplets,  $r_{d,num}$ , are compared in Fig. 3 with the reported numerical values,  $r_{d,ref}$ , by Hua et al. [22]. This comparison is for the following conditions: (a)  $Q_c = 15 - 118 \mu\text{l/s}$  (or  $Ca_c = 0.03-0.225$ ), spanning the dripping and jetting regimes, and,  $Q_d = 0.98 \mu\text{l/s}$ ; (b)  $R_d = 80 \mu\text{m}$  and  $R_c = 300 \mu\text{m}$ ; (c)  $\rho_d = 1000 \text{ kg/m}^3$   $\rho_c = 800 \text{ kg/m}^3$ ; (d)  $\mu_d = 0.031 \text{ Pa}\cdot\text{s}$  and  $\mu_c = 0.047 \text{ Pa}\cdot\text{s}$  and (e)  $\sigma_{d,c} = 98 \text{ mN/m}$ . As shown in Fig. 3, and later in Figs. 4 and 5, the poly-disperse droplets in the dripping regime form at the intermediate values of the continuous liquid's capillary numbers,  $Ca_c$  (or the disperse droplet radius), while the formation of mono-disperse droplets in the same regime prevails at low capillary numbers (or large disperse droplet radius). At high values of  $Ca_c$ , the jetting regime prevails, producing smaller poly-disperse droplets. The transition from the dripping to the jetting regime in Fig. 3 is calculated to occur at  $Q_c = 78 \mu\text{l/s}$  (or  $\bar{u}_c = 0.31 \text{ m/s}$ ), the same as those reported by Hua et al. [22]. The good agreement in Fig. 3 confirms the soundness of the present numerical methodology and the fidelity of the simulations.

In addition to the jetting regime, the processes of forming disperse droplets in the dripping regime (Fig. 1) are successfully simulated. In this regime, the inertia of the disperse liquid flow is much smaller than the interfacial tension (or  $We_d \ll 1$ ). Unlike in the dripping regime, disperse droplets produced in the jetting regime are much smaller and highly poly-disperse. Though poly-disperse droplets also form in the dripping regime, the number and total volume of the satellite droplets are much smaller than in the jetting regime (Fig. 3). The droplets in the poly-disperse dripping regime are highly mono-disperse when total volume of satellites is small.

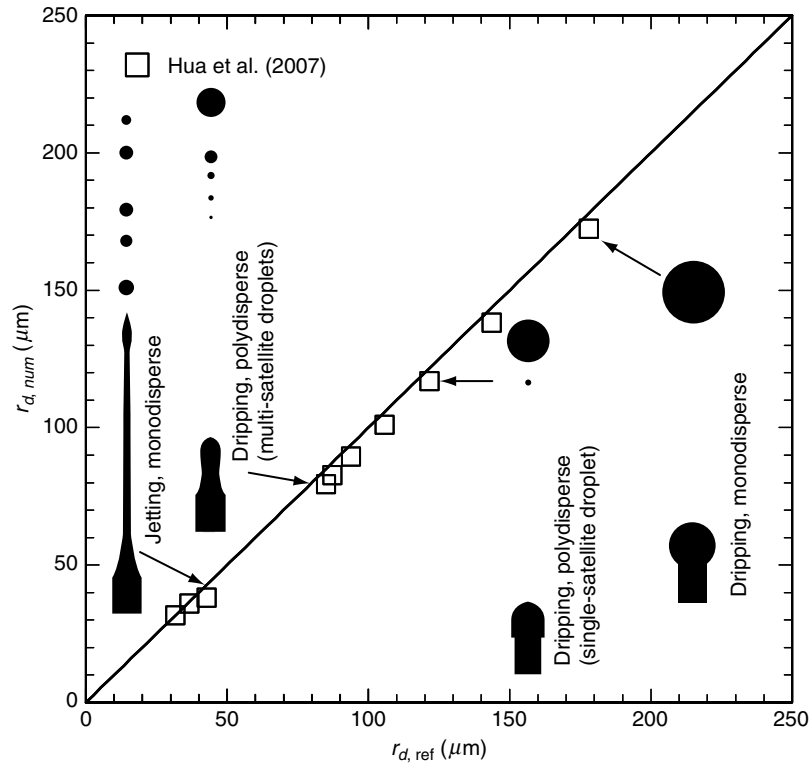


Figure 3. Comparisons of present numerical calculations of radius of disperse droplets with those of Hua et al. [22] for co-flowing immiscible liquids.

While the present numerical methodology is capable of simulating both the dripping and jetting regimes for forming disperse droplets, the results presented and discussed next are only for the formation of mono-disperse and poly-disperse droplets in the dripping regime. The numerical results of a performed parametric analysis, covering wide ranges of liquid properties and operation conditions (Table 1), discussed in the following subsection, are used to develop semi-empirical correlations of the dimensionless radius and forming frequency of disperse droplets in the dripping regime.

## 5. RESULTS AND DISCUSSION

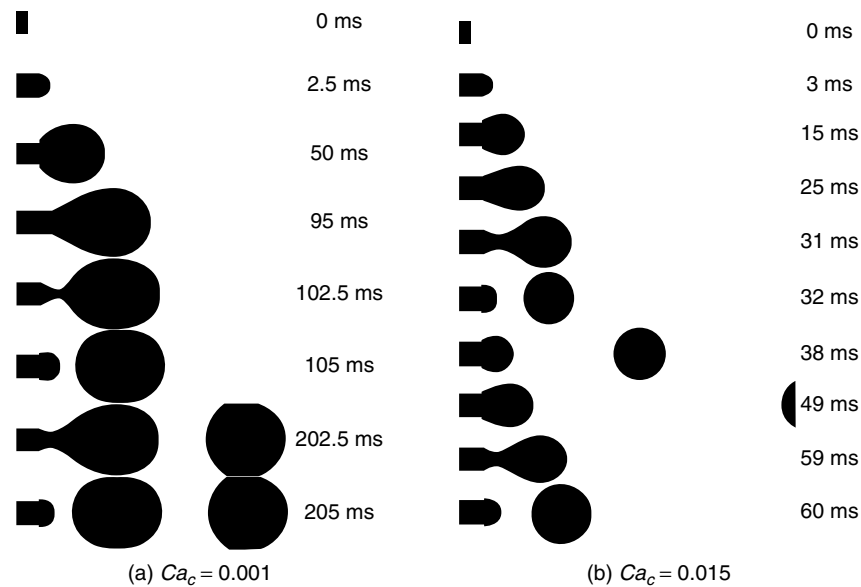
This section presents and discusses the results of the numerical simulations that investigated the effects of various liquids properties and operation parameters on the formation dynamics of the disperse droplets. The parameters considered in the present numerical simulations (Table 1) are:  $\bar{u}_d$ ,  $\bar{u}_c$ ,  $\mu_d$ ,  $\mu_c$ ,  $R_d$ ,  $R_c$ , and  $\sigma_{dc}$ . They varied one at a time, while keeping others at their baseline values listed in Table (2). For poly-disperse droplets in the dripping regime, only the radius of the primary droplet is used in the comparisons presented and discussed in this section and for developing semi-empirical correlations for the radius and forming frequency of the disperse droplets .

### 5.1. Formation of mono-disperse droplets

The images in Figs. 4a and 4b illustrate the evolution of disperse droplets during their successive stages of formation in the dripping regime at two different values of  $Ca_c$ . The images in these figures are for the following parameters:  $R_d = 50 \mu\text{m}$ ,  $R_c = 160 \mu\text{m}$  ( $R^* = 3.2$ ),  $Q_d = 0.24 \mu\text{l/s}$  and  $Re_d = 0.1$ , but  $Q_c = 0.21 \mu\text{l/s}$ ,  $Ca_c = 0.001$  and  $Re_c = 0.02$  in Fig. 4a, and  $Q_c = 3.21 \mu\text{l/s}$ ,  $Ca_c = 0.015$ , and  $Re_c = 0.3$  in Fig. 4b. At these conditions, mono-disperse droplets form in the dripping regime. Though the thickness of the

Table 2. Base values of properties and parameters in performed numerical simulations.

Analysis Parameter	Value	Units
Inner micro-tube radius, $R_d$	100	$\mu\text{m}$
Outer micro-tube radius, $R_c$	1020	$\mu\text{m}$
Disperse liquid rate/injection velocity, $Q_d / \bar{u}_d$	0.97 / 0.031	$\mu\text{l/s} / \text{m/s}$
Continuous liquid rate/ injection velocity, $Q_c / \bar{u}_c$	100 / 0.031	$\mu\text{l/s} / \text{m/s}$
Disperse / Continuous liquid viscosity, $\mu_d / \mu_c$	0.031 / 0.031	Pa·s
Disperse / Continuous liquid density, $\rho_d / \rho_c$	1000 / 1000	$\text{kg/m}^3$
Interfacial tension, $\sigma_{d,c}$	0.096	N/m
Disperse liquid Capillary number, $Ca_d$	0.01	—
Continuous liquid Capillary number, $Ca_c$	0.01	—
Disperse liquid Weber number, $We_d$	0.002	—
Micro-tubes radii ratio, $R^* (R_c/R_d)$	10.2	—
Disperse liquid Reynolds number, $Re_d$	0.2	—
Continuous liquid Reynolds number, $Re_c$	1.8	—

Figure 4. Successive Images of the cyclical formation of mono-disperse droplets in the dripping regime at two different values of  $Ca_c$ .

inner micro-tube wall ( $R_{d,0} - R_d$ ) has a negligible effect on the disperse droplet radius, it may affect the initial development of the disperse liquid pendant forming at the tip of the micro-tube.

As demonstrated in Figs. 4a and 4b, the flat interface located initially midway inside the inner micro-tube (at  $t = 0$ ) acquires a parabolic shape and then moves forward, driven by the constant injection of the disperse liquid, to the tip of the inner micro-tube. When a parabolic interface emerges from the tip of the inner micro-tube ( $\leq 3$  ms into the simulated transient, Figs 4a and 4b), the combined effect of the disperse liquid inertia and the interfacial tension,  $\sigma_{d,c}$ , cause the parabolic interface to evolve into a disperse spherical pendant that steadily grows in size with time. This occurs in Figs. 4a and 4b after  $\sim 50$  ms and  $\sim 15$  ms, respectively, from the start of the transient.

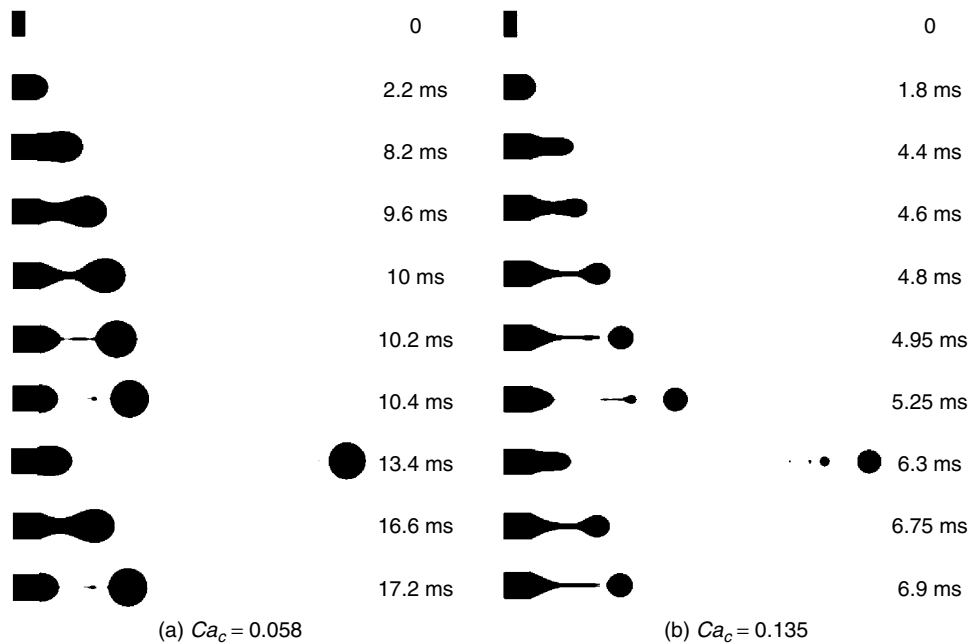


Figure 5. Successive Images of the cyclical formation of poly-disperse droplets in the dripping regime at two different values of  $Ca_c$ .

As the disperse liquid pendent grows in size, the interfacial tension increasingly dominates the shape and movement of its surface. The induced viscous drag by the continuous liquid flow on the moving surface of the disperse droplet accelerates its forward motion, and then initiates necking close to the tip of the inner micro-tube (at  $\sim 100$  ms and 31 ms in Figs. 4a and 5b). Eventually, a pinch off of the disperse droplet occurs close to the tip of the inner micro-tube, and a second cycle (at  $\sim 105$  ms and 32 ms in Figs. 4a and 4b, respectively) for forming a disperse droplet begins.

In Fig. 4a, the growing disperse droplet constrained by the wall of the outer micro-tube begins to elongate axially at  $\sim 95$  ms into its formation cycle. In Fig. 4b, however, the growing droplet remains perfectly spherical and not constrained by the outer micro-tube wall. The forming cycle of the disperse droplets, for the conditions in Figs. 4a and 4b, repeats at an average frequency of 10 and 36 Hz, respectively, excluding the first droplet. With the fine mesh numerical grid used in the present simulations no numerical instabilities are encountered during the formation cycle of the disperse droplets, including pinch off.

## 5.2. Formation of poly-disperse droplets

Increasing the injection rate of the continuous liquid,  $Q_c$ , to  $12.3 \mu\text{l/s}$  (or  $Ca_c$  to 0.058) and  $28.9 \mu\text{l/s}$  (or  $Ca_c$  to 0.135) decreases the radius of the mono-disperse droplet and increases its frequency of formation to 147 and 513 Hz, respectively, excluding the first droplet (Figs 5a and 5b). Increasing the injection rate of the continuous liquid also extends the fine thread of the disperse liquid connecting the growing droplet to the liquid cone at the tip of the inner micro-tube, before pinch off (Figs. 5a and 5b).

The interfacial shear exerted by the continuous liquid flow at high injection rates develops a thread of the disperse liquid that extends axially, while the droplet is in the static growth stage. This occurs in Figs. 5a and 5b at 8.2 ms and 4.4 ms in the simulation cycle of the disperse droplet. Following the droplet's pinch off at the end of the extended disperse liquid thread, the thread retracts to the tip of the inner micro-tube. Shortly thereafter, another disperse droplet begins to grow into the continuous liquid co-axial flow. The length of the disperse liquid thread increases as the

flow rate of the continuous liquid increases. Following the primary droplet's pinch off, the disperse liquid thread breaks up into (Figs. 5a and 5b) one or more satellite droplets of very smaller radii (Fig. 5b). The process depicted in Fig. 5b for forming disperse liquid droplets is referred to as poly-disperse dripping regime, while that presented in Figs. 4a and 4b is referred to as mono-disperse dripping regime.

At low disperse liquid injection rates, the internal circulation of the liquid in the forming droplet (Fig. 6) negligibly affects its pinch off radius and formation frequency. On the other hand, such liquid circulation would enhance mixing with other additives for drug delivery applications or altering the microstructure of produced solid micro-spheres. Increasing the injection rate of disperse liquid increases the formation frequency, by not the radius of the droplet; more on that in section 5.4.6.

The images presented in Figs. 4 and 5 clearly demonstrate the effect of increasing the injection rate,  $Q_d$ , or Capillary number of continuous liquid,  $Ca_c$ , on the formation dynamics of the disperse droplets. The radius and forming frequency of the disperse droplet also depend on the values of other parameters including the physical properties of the two immiscible liquids, interfacial tension and radii of the co-axial micro-tubes (Fig. 2). The following subsections present and discuss results of the effects of these parameters individually on the formation dynamics and frequency and the radius of mono-disperse and poly-disperse droplets in the dripping regime.

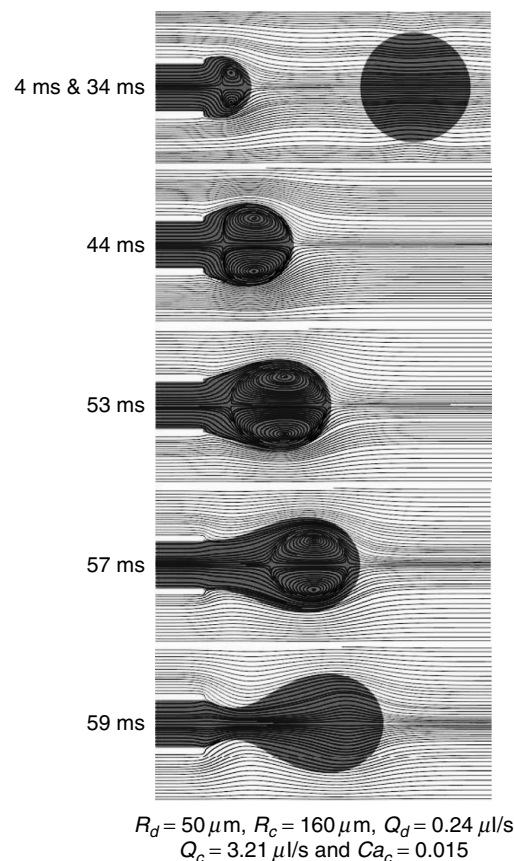


Figure 6. Flow circulation inside disperse droplet, during its successive stages of formation, produces clockwise and counter-clockwise vortices.

### 5.3. Flow field inside disperse droplets

The images shown in Fig. 6 are of the flow fields inside a mono-disperse droplet and of the surrounding co-axial continuous liquid at different times during the simulated formation cycle of the droplet, at  $Ca_c = 0.015$ . As soon as a disperse spherical pendent appears at the tip of the inner co-axial micro-tube, a pair of clockwise and counter-clockwise vortices forms inside the liquid pendent. This is shown in Fig. 6 after 4 and 34 ms into the transient or formation cycle of the disperse droplet. The extent of the internal liquid vortices increases as the droplet continues to grow. The vortices are driven by the change in the local curvature (or surface tension force) along the surface of disperse droplet.

The curvature of the interface is positive and highest at the leading tip of the ellipsoidal droplet, while the local surface curvature is the lowest, either zero (flat interface) or negative (concave interface), near the tip of the inner micro-tube where necking occurs. As a result, the disperse liquid, starting at the leading tip of the disperse droplet, flows backward along the centerline. At the tail end of the droplet, the liquid flow reverses direction and splits into two vortices (a clockwise top vortex and a counter-clockwise bottom vortex). In the necking phase of the growing droplet, these vortices increase in size, but diminish in the pinched off spherical droplet. This is illustrated in Fig. 6 by the large spherical image at 34 ms. The internal circulation of the disperse liquid ceases in the pinched off spherical droplet because of the uniformity of the surface curvature, and hence the surface tension force along its surface (see the mono-disperse droplet in top image in Fig. 6).

The following subsection presents the results of a parametric analysis that investigated the effects of various properties of disperse and continuous liquids and radii of co-axial micro-tubes on the radius and forming frequency of the disperse droplets. The obtained results, for wide ranges of liquids properties and operating parameters (Table 1), are used in section 5.5 to develop semi-empirical correlations for the dimensionless radius and formation frequency of the disperse droplets.

### 5.4. Parametric analysis

In the performed parametric analysis, the following parameters varied one at a time:  $R_d$ ,  $R_c$ ,  $\sigma_{d,c}$ ,  $\mu_d$ ,  $\mu_c$ , and  $\bar{u}_d$ . This section presents and discusses the results of the effects of these parameters on the formation dynamics and radius of disperse droplet as a function of the Capillary number of the continuous liquid,  $Ca_c$ . The collective results of the performed parametric analysis are used to develop semi-empirical correlations for the dimensionless radius and formation frequency of the disperse droplets in terms of  $Ca_c$  and the ratios of Reynolds numbers and micro-tube radii of the two immiscible co-flowing liquids.

In this analysis, the value of  $Ca_c$  varied only by varying the injection velocity of the continuous liquid. However, for same value of  $Ca_c$  reached by varying other properties (e.g., the interfacial tension,  $\sigma_{d,c}$ , or the continuous liquid viscosity,  $\mu_c$ ) the diameter of the disperse droplet will be different (see results in subsections 5.4.4 and 5.4.5).

#### 5.4.1. Continuous liquid micro-tube radius

The results of the effects of the micro-tube diameter and Capillary number of the continuous liquid on the dimensionless radius of the forming disperse droplets are presented in Fig. 7. These results are for  $R_c = 320 \mu\text{m}$ ,  $520 \mu\text{m}$  and  $1020 \mu\text{m}$  (or  $R^* = 3.2$  (solid circles),  $5.2$  (open triangles) and  $10.2$  (open squares)), respectively. Fig. 7 shows that the dimensionless radius of the disperse droplet decreases slowly with increasing  $Ca_c$  (or injection velocity of the continuous liquid) up to that corresponding to  $r_d^* = 0.5 R^*$  (or  $r_d = 0.5 R_c$ ). Below this value  $Ca_c$ , which depends on the radius of the continuous liquid micro-tube, the dimensionless radius of the forming disperse droplet,  $r_d^*$ , decreases inversely proportional to  $\sqrt{Ca_c}$ .

Decreasing the radius of the continuous liquid micro-tube,  $R_c$ , decreases that of the forming disperse droplet. This is because, for the same injection velocity of the continuous liquid, decreasing its micro-tube radius increases the interfacial drag exerted onto the surface of the growing disperse droplet. Eventually, this effect causes the droplet to pinch off at a smaller radius. The smaller droplet radius is typically associated with a higher frequency of formation.

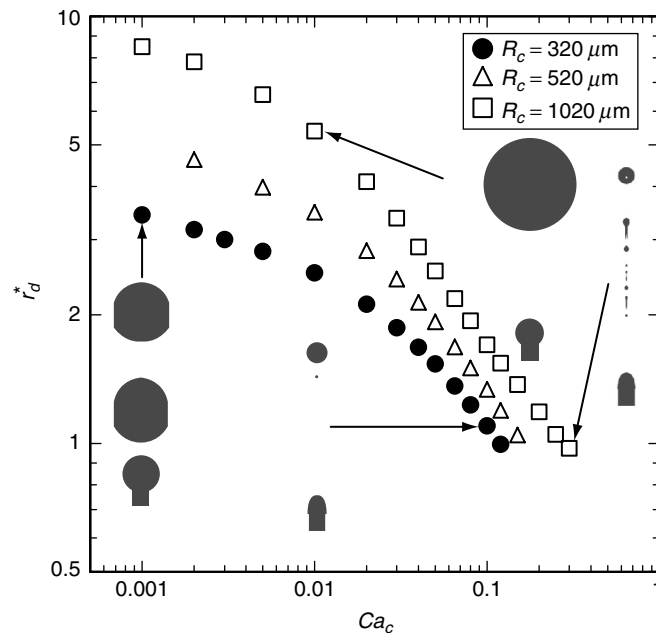


Figure 7. Effects of micro-tube radius and Capillary number of continuous liquid on dimensionless radius of disperse droplet.

The results delineated in Fig. 7 also show that for  $Ca_c \leq 0.01$ , the mono-disperse dripping regime prevails and relatively large droplets form one at a time at a relatively low frequency. At higher values of  $Ca_c$ , the resulting emulsion becomes poly-disperse. The primary droplet's pinch off is followed by the formation of one or several small satellite droplets. As shown in Fig. 7, at  $Ca_c \sim 0.3$ , the number and the collective size of the satellite droplets could affect the radius and the formation frequency of the larger, primary droplet.

#### 5.4.2. Formation frequency

The calculated frequencies of forming disperse droplets in the dripping regime at different values of  $Ca_c$  and radii of the continuous and the disperse liquids micro-tubes,  $R_c$  and  $R_d$ , are compared in Figs. 8a and 8b. These Figures plot the formation frequency, determined from dividing the volumetric flow rate of the disperse liquid by the volume of the formed disperse droplet,  $f_{mb}$ , versus that determined from the transient progression in the numerical simulation,  $f$ .

For mono-disperse droplets that occur at low  $Ca_c$ , the two frequencies are identical. However, for the poly-disperse droplets in the dripping regime, occurring at high  $Ca_c$ ,  $f_{mb}$  of the primary droplet becomes progressively higher than  $f$  with increased  $Ca_c$ . This is because only the volume of the primary droplet is considered, and the cumulative volume of the satellite droplets, which increase with  $Ca_c$ , is neglected in the determination of  $f_{mb}$  (Figs. 8a and 8b). The results in these figures show that the values of the formation frequencies and the difference between  $f_{mb}$  and  $f$ , depends on the radii of micro-tubes of the disperse and continuous co-axial flowing liquids.

The results in Fig. 8a are for  $R_d = 50$  and  $R^* = 3.2, 6.4$  and  $10.2$ , while those in Fig. 8b are for  $R_d = 100$  and  $R^* = 3.2, 5.2$  and  $10.2$ . For same  $R_c$ , decreasing  $R_d$  (or increasing  $R^*$ ) increases the formation frequency of the mono-disperse liquid droplets up to 200 and 100 Hz in Fig. 8a and 8b, respectively. For poly-disperse droplets in the dripping regime, the formation frequency could be much higher;  $> 200$  and 100 Hz, in Figs. 8a and 8b, respectively.

The comparisons in Figs. 8a and 8b confirm the accuracy of determining the formation frequency of the mono-disperse droplet by dividing the flow rate of the disperse liquid by the volume of the forming

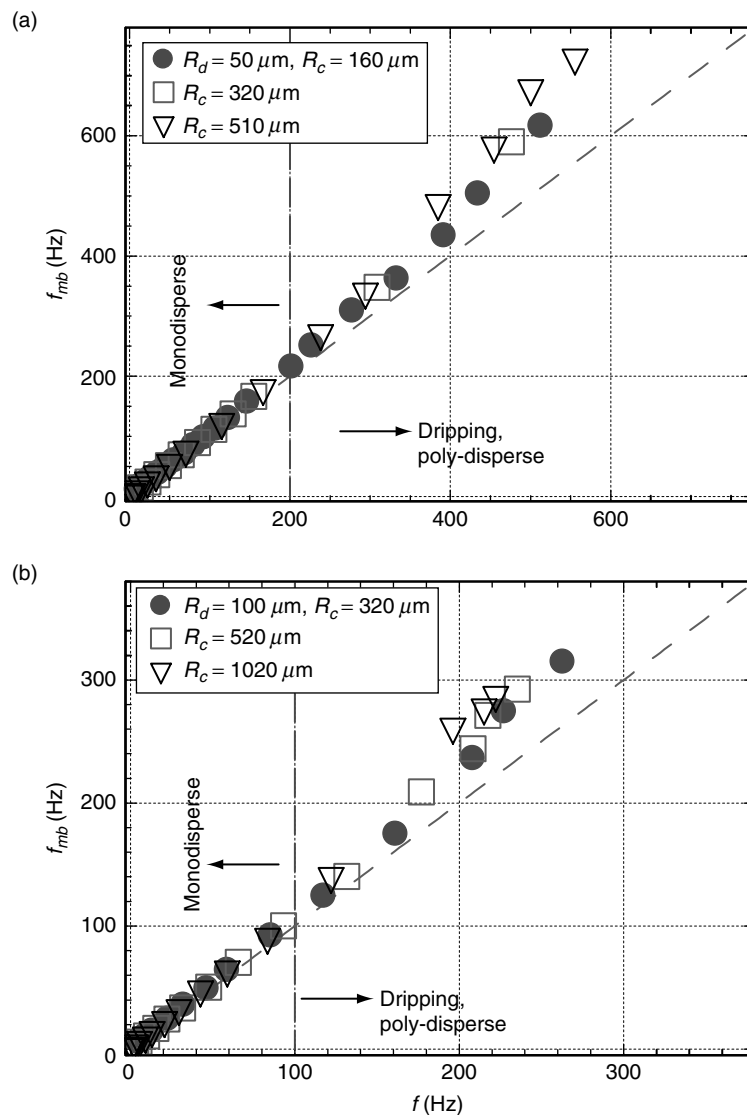


Figure 8. Effects of radii of micro-tubes of disperse and continuous liquids on formation frequency of disperse droplets in dripping regime.

droplet. This simple method is also accurate for determining the formation frequency of the primary droplets in the poly-disperse dripping regime. For this condition, which prevails in Figs. 8a and 8b up to 350 and 160 Hz, respectively, the difference between  $f_{mb}$  and  $f$  for the primary droplets in the poly-disperse dripping regime is negligibly small.

#### 5.4.3. Disperse liquid micro-tube radius

The results on the effects of the radius of disperse liquid micro-tube and the continuous liquid Capillary number,  $Ca_c$ , on the dimensionless radius of the disperse droplet are presented and compared in Figs. 9a and 9b. The results are for two different radii of the disperse liquid micro-tube ( $R_b = 50 \mu\text{m}$  and  $100 \mu\text{m}$ ), but same radius of the continuous liquid micro-tube,  $R_c = 320 \mu\text{m}$ . The dimensionless radius of the disperse droplet in Fig. 9a,  $r_c^*$ , is based on that of the continuous liquid micro-tube, while that in Fig.

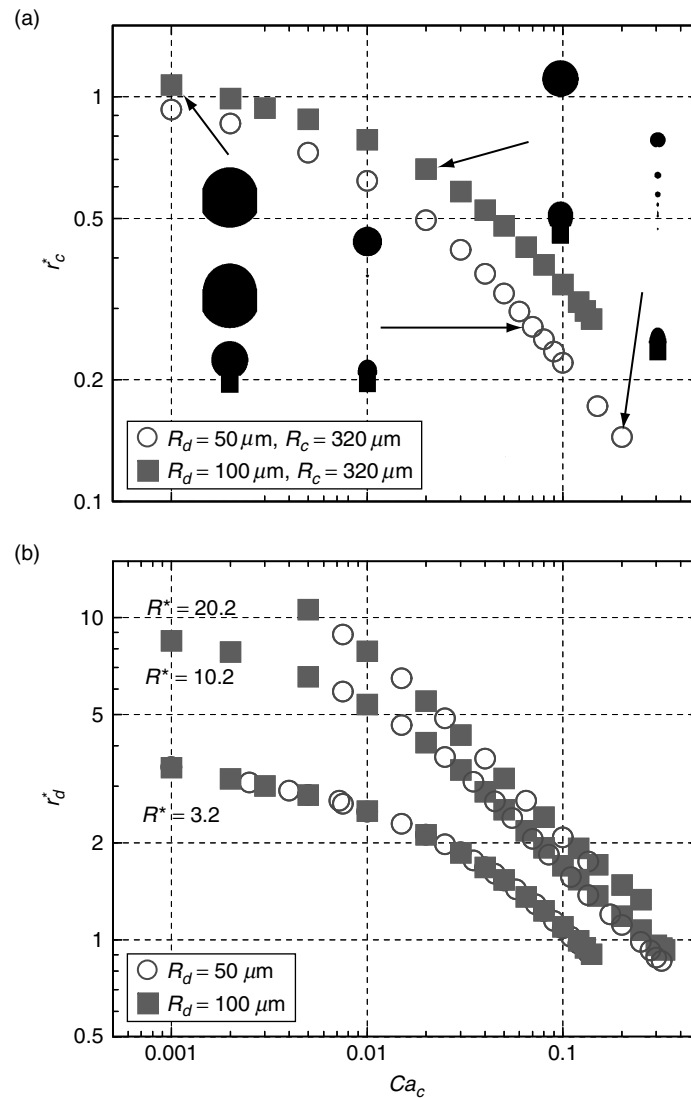


Figure 9. Effects of disperse liquid micro-tube radius and continuous liquid Capillary number on the radius of forming disperse droplet in dripping regime.

9b,  $r_d^*$  is based on the radius of the disperse liquid micro-tube. In Fig. 9a, when  $r_c^* \leq 0.5$ , it decreases inversely proportional to square root of the continuous liquid Capillary number,  $\sqrt{Ca_c}$ . The decrease in  $r_c^*$  with increasing  $Ca_c$ , is more pronounced for the small disperse liquid micro-tube radius. At lower values of  $Ca_c$ ,  $r_c^*$  increases slower and the effect of  $R_d$  on the radius of the forming disperse droplets gradually diminishes with decreasing  $Ca_c$  (Fig. 9a). Generally, for same  $Ca_c$ , increasing the radius of disperse liquid micro-tube,  $R_d$ , increases that of the forming disperse droplet (Fig. 9a).

For the same radii ratios of the disperse and continuous liquids micro-tubes,  $R^*$ , the dimensionless droplet radius, based on that of the inner micro-tube,  $r_d^*$ , is independent of the radius of the disperse liquid micro-tube,  $R_d$ , but decreases with increasing  $Ca_c$  (Fig. 9b). The results in this figure also show that for the same  $Ca_c$ , increasing  $R^*$  (or radius of continuous liquid micro-tube,  $R_c$ ) increases the dimensionless radius of the forming disperse droplet,  $r_d^*$ .

In addition to the geometrical effects shown in Figs. 7–10, the physical properties of the co-axial flowing immiscible liquids, including the interfacial tension and the viscosities affect both the frequency and the radius of the disperse droplets. The results demonstrating the effect of the interfacial tension,  $\sigma_{d,c}$ , are presented in Fig. 10 and discussed next.

#### 5.4.4. Interfacial tension

The results presented in Figs. 10a – 10c are for the same radius of disperse liquid micro-tube,  $R_d = 50 \mu\text{m}$ , but three different values of  $R_c$  and  $\sigma_{d,c}$ . The interfacial surface tension is already included in the definition of  $Ca_c$  ( $\mu_c \bar{u}_c / \sigma_{d,c}$ ), thus the results in these figures show how the interfacial surface tension, beyond that already included in  $Ca_c$ , affects the radius of the forming droplet,  $r_d^*$ . This additional effect is negligibly small. In general, at the same  $Ca_c$  increasing the interfacial tension decreases the radius of the disperse droplet, depending on the value of  $R_c$ . When  $R_c = 160 \mu\text{m}$  (or  $R^* = 3.2$ ), increasing the interfacial tension almost 5 times, from 20 to 96 mN/s, decreases the radius of the forming disperse droplet,  $r_d^*$ , by only  $\sim 20\%$  (Fig. 10a).

When increasing  $R_c$  to 320 and 510  $\mu\text{m}$  (or  $R^* = 6.4$  (Fig. 10b) and 10.2 (Fig. 10c)), respectively, the effect of interfacial tension on the droplet radius becomes progressive smaller. For example, the results in Fig. 10c (for  $R^* = 10.2$  or  $R_c = 510 \mu\text{m}$ ) show that for the same  $Ca_c$ , increasing  $\sigma_{d,c}$ , from 20 to 96 mN/s decreases the radius of the forming disperse droplet by only 5%. Figures 10a–10c also show that for the same  $Ca_c$ , the additional effect of increasing interfacial tensions diminishes at  $Ca_c \geq 0.1$ .

To present the total effect of the interfacial tension on the radius of the forming disperse droplet,  $r_d^*$ , the results in Figs. 10a–10c are shown in Figs. 10d–10f, respectively, by plotting  $r_d^*$  versus the ratio of the average injection velocities of the continuous and disperse liquids,  $\bar{u}_c / \bar{u}_d$ . The results in Figs. 10d–10f clearly show that increasing either the interfacial tension,  $\sigma_{d,c}$ , or the average injection velocity of the continuous liquid,  $\bar{u}_c$ , decreases the dimensionless radius of the disperse droplet,  $r_d^*$ . The next section presents the results on the effects of the dynamic viscosities of the disperse and continuous liquids on the radius of forming disperse droplets in the dripping regime.

#### 5.4.5. Dynamic viscosities of disperse and continuous liquids

The results in Figs. 11 and 12 show the effects of changing the dynamic viscosities of the disperse and continuous liquids,  $\mu_d$  and  $\mu_c$ , on the radius of the forming droplets in the dripping regime. Fig. 11 shows that increasing the viscosity of the disperse liquid only slightly decreases the radius of the forming droplets. Such an increase in disperse liquid viscosity slows down the growth rate of the droplet, but increases the rate of momentum transfer to the interface. The combined effect initiates earlier necking and smaller droplets pinch off (Fig. 11).

Conversely, increasing the dynamic viscosity of the continuous liquid,  $\mu_c$ , (or  $Ca_c$ ) increases the drag exerted onto the surface of the growing disperse droplet, delaying its necking and pinch-off. Thus, the radius of the disperse droplet increases with increased viscosity of the continuous liquid (Figs. 12a and 12b). In general, the dynamic viscosity of the continuous liquid has a larger effect than that of the disperse liquid on the radius of the forming droplet, at the same  $Ca_c$ .

The effect of changing the viscosity of either the continuous or disperse liquid on the radius of the forming disperse droplet decreases with increasing  $Ca_c$ . Increasing the viscosity of the disperse liquid (Fig. 11) or decreasing that of the continuous liquid (Figs. 12a and 12b) decreases the radius of the disperse droplet, however, the decrease is relatively small. For example, the results in Fig. 11 show that for the same  $Ca_c$  increasing the disperse liquid viscosity  $\sim 16$  times, from 0.0078 to 0.124 Pa.s, decreases the radius of the forming disperse droplet by less than 25%. Conversely, the results in Fig. 12a show that for the same  $Ca_c$  increasing the viscosity of the continuous liquid  $\sim 16$  times, from 0.0078 to 0.124 Pa.s, increases the size of the forming disperse droplet by about 44%, at  $Ca_c < 0.08$  and slightly less at higher values of  $Ca_c$ .

To show the total effect of the continuous liquid viscosity, the results in Fig. 12a are plotted in Fig. 12b in terms of the ratio of the average injection velocities of the continuous and disperse liquids.

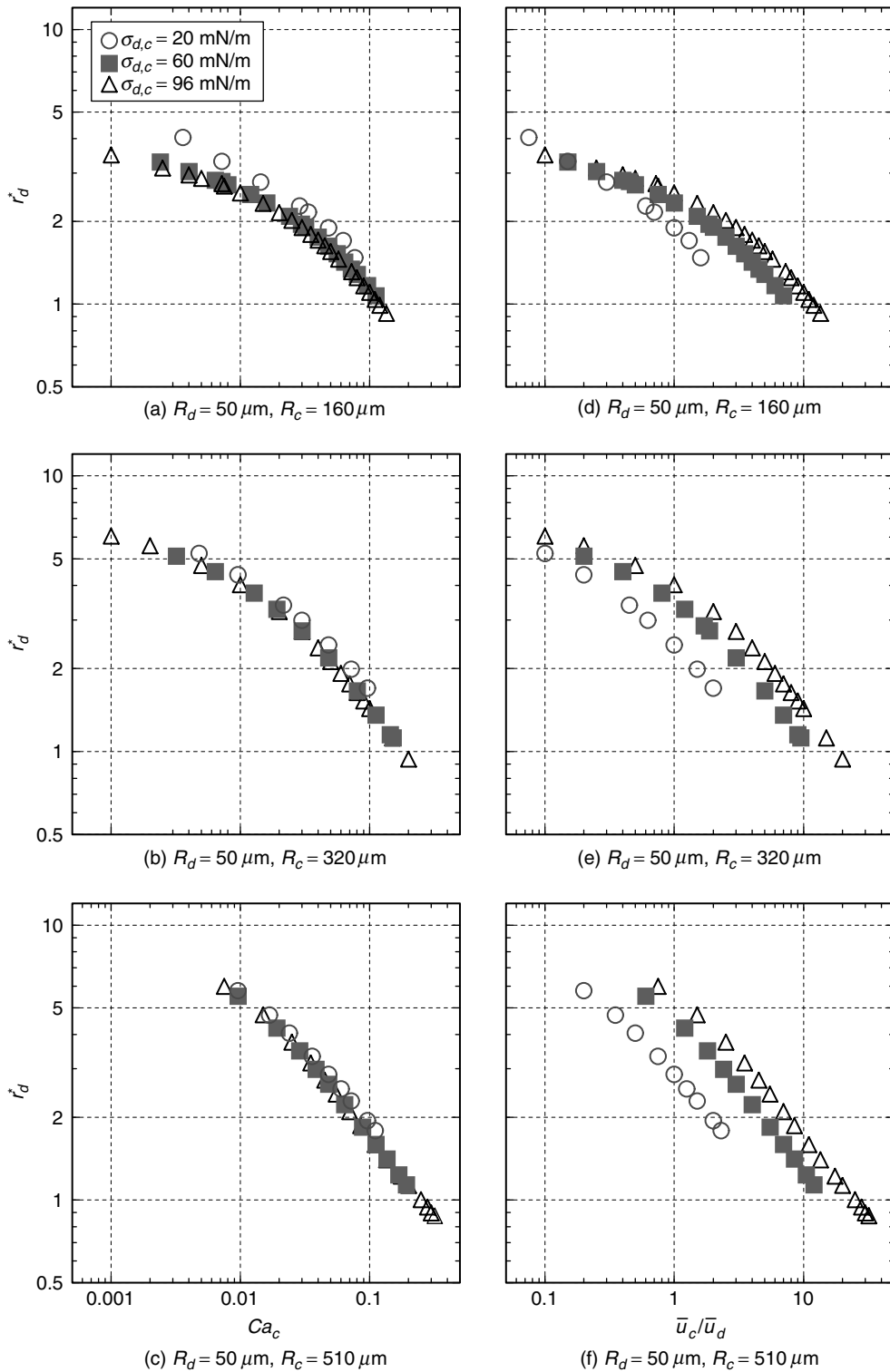


Figure 10. Effects of continuous liquid micro-tube radius and interfacial tension on radius of forming disperse droplets in the dripping regime.

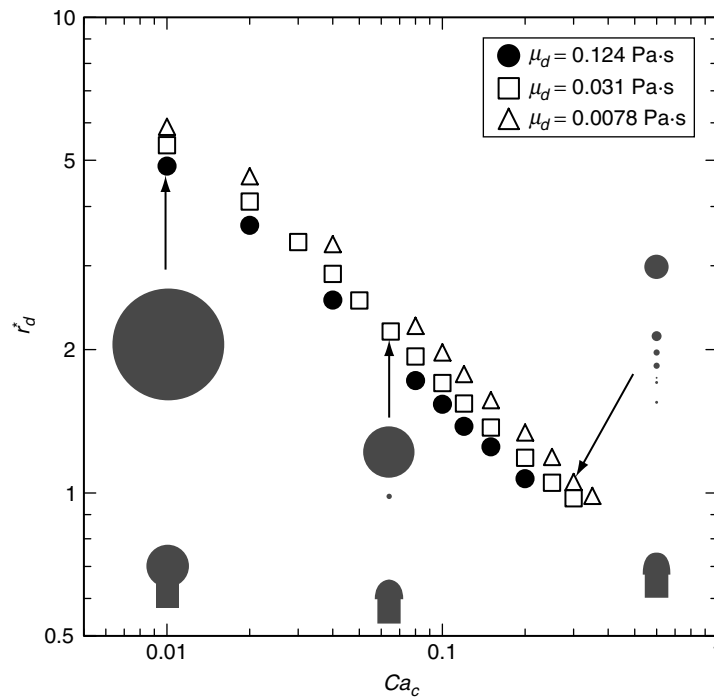


Figure 11. Effects of disperse liquid viscosity and continuous liquid Capillary number on radius of forming droplets in the dripping regime.

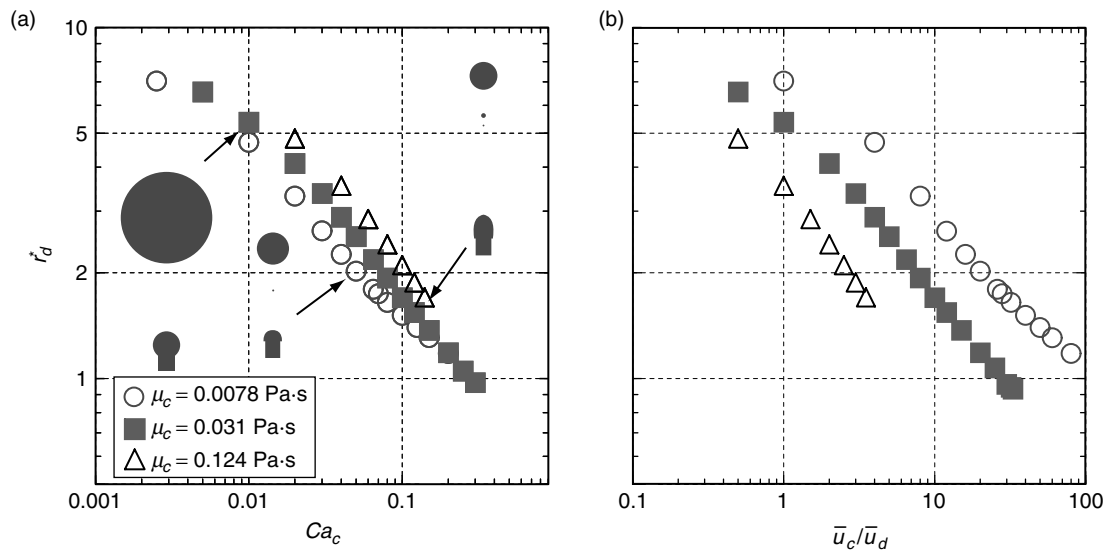


Figure 12. Effects of continuous liquid's viscosity and Capillary number on radius of disperse droplets in the dripping regime.

Fig. 12b shows that the continuous liquid viscosity strongly affects the radius of the forming droplets. Increasing the continuous liquid viscosity significantly increases the radius of the disperse droplets in the dripping regime.

The results presented in Figs. 7–12 show a strong dependence of the radius of the disperse droplet on the injection rate or the capillary number of the continuous liquid,  $Ca_c$ . In the present analysis, the injection rate of the disperse liquid are relatively very low ( $We_d$  is  $\ll 1.0$ ). The obtained results of the effect of the injection rate of the disperse liquid (Table 1) on both the radius and frequency of the forming droplets are presented and discussed next (Figs. 13a and 13b).

5.4.6. Disperse liquid injection rate

Unlike the injection rate of the continuous liquid, that of the disperse liquid insignificantly affects the size of the forming disperse droplets in the dripping regime (Fig. 13a). This is because disperse liquid injection rates used in the present analysis (Tables 1) are low ( $We_d \ll 1$ ). The results in Fig. 13a show

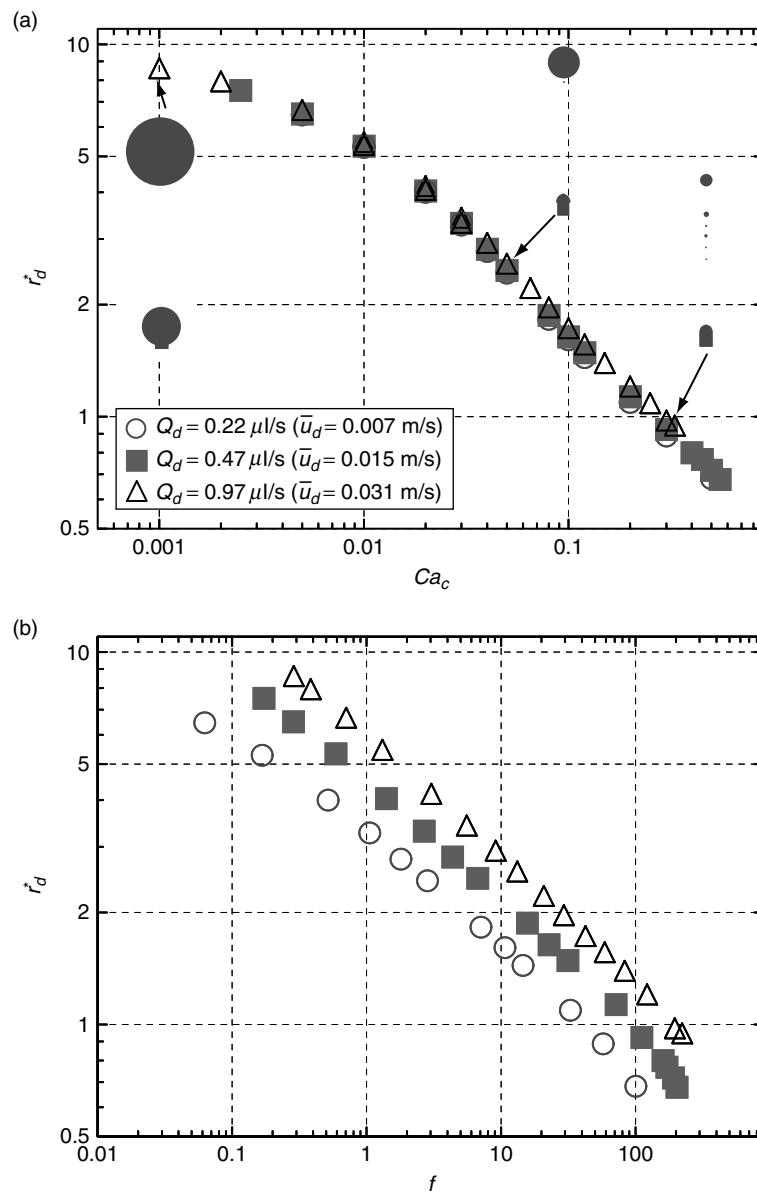


Figure 13. Effects of disperse liquid injection rate on droplet’s radius and frequency.

that increasing the injection rate of the disperse liquid by 4.4 times, from 0.22 to 0.97  $\mu\text{l/s}$ , increases the radius of the disperse droplet by less than 10%. Results also show that increasing  $Ca_c$  markedly decreases the radius of the forming disperse droplet. For example, when  $Ca_c = 0.001$  the radius of the disperse droplet is as much as 8.5 times that of the inner micro-tube ( $r_d^* = 8.5$ ), but almost the same as that of the inner micro-tube ( $r_d^* = 1.0$ ) when  $Ca_c \sim 0.3$  (Fig. 13a).

The radius of the disperse droplet is inversely proportional to its formation frequency (Fig. 13b). Although increasing the injection rate of the disperse liquid has little effect on the radius of the forming droplets (Fig. 13a), it generally increases their formation frequencies. For example, the results in Fig. 13b show that for a droplet radius that is twice that of the inner micro-tube ( $r_d^* = 2.0$ ), increasing the injection rate of the disperse liquid from 0.22 to 0.97  $\mu\text{l/s}$  increases the frequency of forming this droplet from  $\sim 6$  to 30 Hz. When halving the droplet size ( $r_d^* = 1.0$ ) the formation frequency increases from  $\sim 40$  to as much as 200 Hz, respectively.

### 5.5. Correlations for disperse droplets

The results of the present parametric analysis quantified the effects of the various operation parameters and the physical properties of the disperse and continuous liquids on both the radius and forming frequency of disperse droplets in the dripping regime. The compiled results of the analysis are used to develop semi-empirical correlations of the dimensionless radius and forming frequency of the disperse droplets in the dripping regime. These correlations, presented and discussed next, are valid for the ranges of liquids properties and operation parameters listed in Table 1 and the dimensionless quantities in Fig. 14.

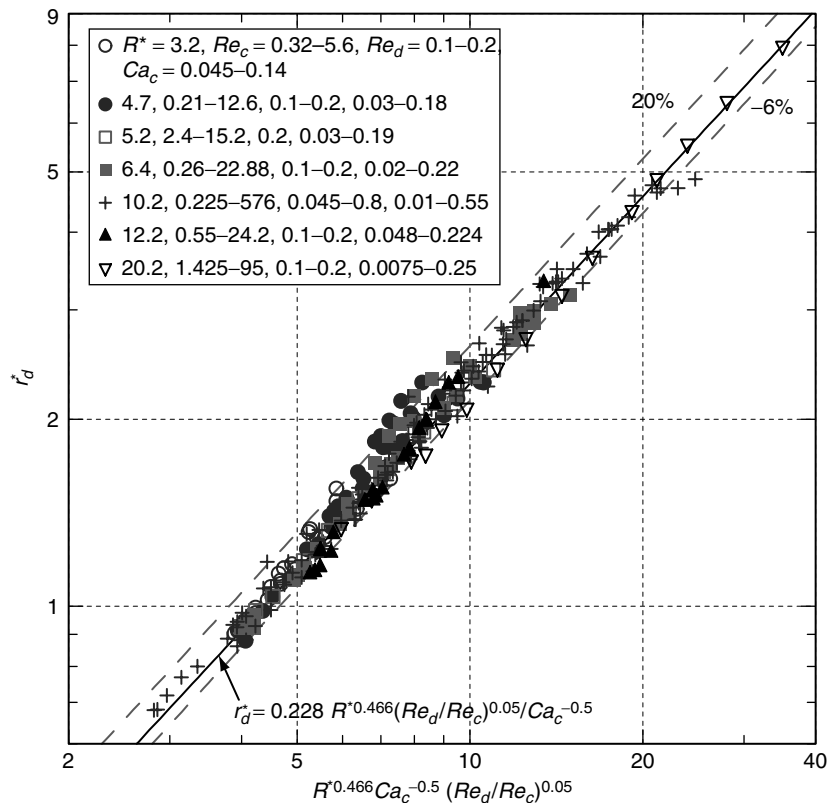


Figure 14. Comparison of semi-empirical correlation (Eq. (11)) with calculated values for dimensionless radius of disperse droplet in dripping regime.

5.5.1. Correlations for disperse droplets radius

The calculated values of the dimensionless radius of the disperse droplet, over wide ranges of liquid properties and parameters (Table 1 and Fig. 14), are correlated as:

$$r_d^* = (r_d / R_d) = 0.228R^{*0.466} (Re_d / Re_c)^{0.05} / (Ca_c^{0.5}) \tag{11}$$

This correlation, for  $r_d^* \leq 0.5 R^*$ , is also applicable for predicting the radius of the primary disperse droplet in the poly-disperse dripping regime. Equation (11) fits the numerical results to within +20% to -6% (Fig. 14). The dimensionless radius of the droplet strongly depends on the ratio of the radii of the co-axial micro-tubes (Fig. 2) and the Capillary number of continuous liquid,  $Ca_c$ . It weakly depends on the ratio of Reynolds numbers of the disperse and continuous liquids.

The exponents of the different dimensionless quantities on the right hand side of Eq. (11), indicate their weighting on the radius of the forming disperse droplet in the dripping regime. The exponent of the Capillary number of the continuous liquid,  $Ca_c$ , is the largest, but negative (- 0.5), followed close second by that of the radii ratio of the continuous and disperse liquid micro-tubes (0.466), and a distance third by the exponent of the Reynolds numbers ratio of these liquids (0.05).

The developed semi-empirical correlation for the dimensionless radius of the disperse droplets in the dripping regime (Eq. (11)) is compared in Fig. 15 with the reported experimental measurements for co-flowing water (disperse liquid) and salad oil (continuous liquid) in co-axial micro-tubes by Gu, Kojima and Miki [17]. This comparison is for the radius of the disperse droplets (water),  $r_d \leq 0.5 R_c$ . Table 3 lists the parameters and liquid properties in the experiments for the co-flowing liquids in the direction of gravity [17].

Equation (11) is within +10% to -14% of the experimental measurements of the radius of the disperse water droplets in a continuous co-flowing salad oil in the dripping regime [17] (Fig. 15). The good agreement between the developed correlation (Eq. (11)) and the experimental measurements

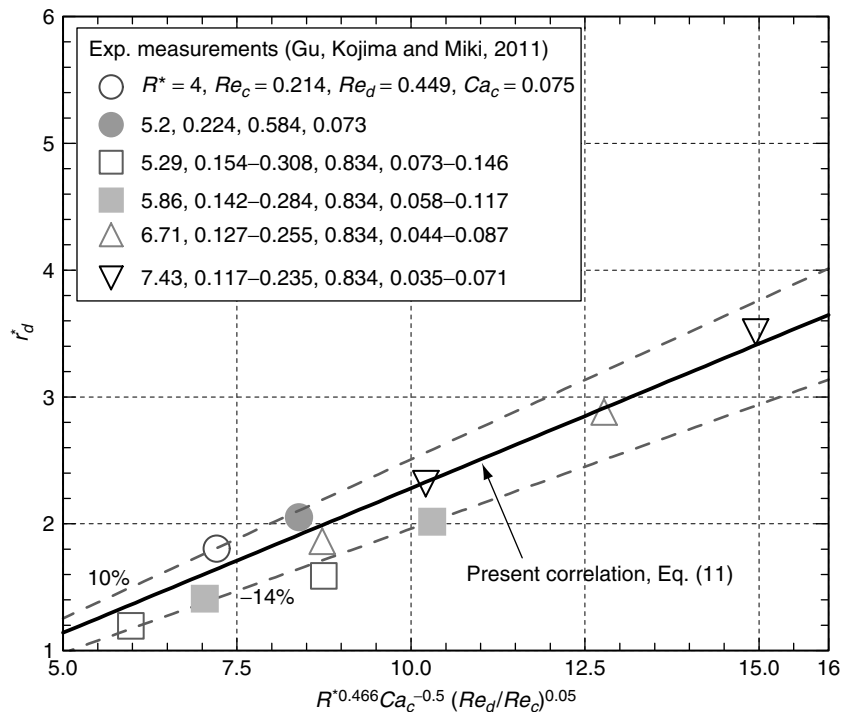


Figure 15. Comparison of semi-empirical correlation (Eq. (11)) with experimental measurements of dimensionless radius of disperse droplets in dripping regime [17].

Table 3. Used parameters and liquids properties in experiments [17].

Analysis Parameter	Value	Units
Inner micro-tube outer radius, $R_{d,o}$	55–85	$\mu\text{m}$
Inner micro-tube wall thickness (assumed)	20	$\mu\text{m}$
Outer micro-tube radius, $R_c$	185–260	$\mu\text{m}$
Water flow rate, $Q_d$	0.046	$\mu\text{l/s}$
Water injection velocity, $\bar{u}_d$	0.0035–0.012	m/s
Salad oil flow rate, $Q_c$	4.167–8.333	$\mu\text{l/s}$
Salad oil injection velocity, $\bar{u}_c$	0.021–0.085	m/s
Water / Salad oil viscosity, $\mu_d / \mu_c$	0.001/0.0675	Pa·s
Water / Salad oil density, $\rho_d / \rho_c$	1000/940	$\text{kg/m}^3$
Interfacial tension, $\sigma_{d,c}$	0.0393	N/m
Disperse liquid Weber number, $We_d$	0.00004–0.00025	—

further validates the methodology used in the present analysis and the fidelity of the numerical simulations.

Based on the validation of the calculations of the dimensionless radius of the disperse droplets in the dripping flow regime, the corresponding values calculated of the dimensionless formation frequency are compiled to develop a semi-empirical correlation (Eq. (12)), presented and discussed next. This

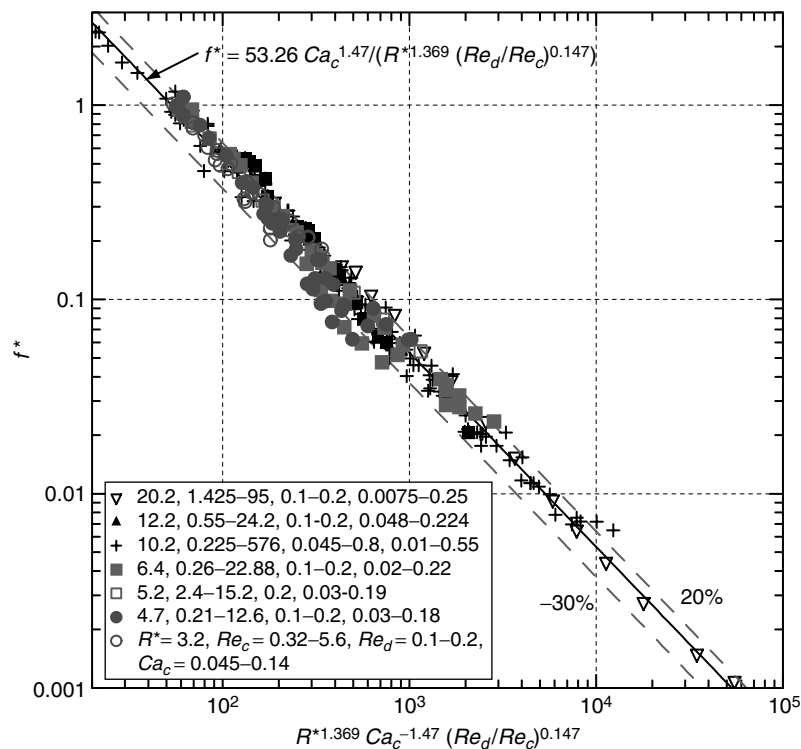


Figure 16. Comparison of semi-empirical correlation (Eq. (12)) with calculated values for dimensionless frequency of forming disperse droplets in dripping regime.

correlation is compared in Fig. 16 with the numerical simulation results of the formation frequency of disperse droplets in the dripping regime.

### 5.5.2. Correlation of forming frequency of disperse droplets

The calculated values of the dimensionless frequency of forming disperse droplets in the dripping regime are correlated, using the same dimensionless quantities on the right hand side of Eq. (11), but in opposite proportionality and with higher exponents (Fig. 16), as:

$$f^* = 53.26 Ca_c^{1.47} / [R^{*1.369} (Re_d / Re_c)^{0.147}] \quad (12)$$

While the dimensionless disperse droplet radius,  $r_d^*$ , increases proportional to the grouping of the dimensionless quantities on the right hand side in Eq. (11), the dimensionless frequency of forming droplets,  $f^*$ , decreases as the total value of the dimensionless quantities on the right hand side of Eq. (12) increases. The respective exponents indicate the weighting of the dimensionless quantities on the right hand side of Eq. (12).

Fig. 16 compares the developed correlation for the dimensionless frequency of forming the disperse droplets in the dripping regime (Eq. (12)), subject to the ranges of parameters listed in Table 1 and shown in Figs. 14 and 16. This correlation is within +20% to -30% of the obtained numerical values of the dimensionless frequency of the disperse droplets.

## 6. SUMMARY AND CONCLUSIONS

This paper numerically investigated the formation dynamics of disperse droplets in the dripping regime for co-flowing immiscible liquids in co-axial micro-tubes. Also investigated are the effects of the different operation parameters and physical properties of the liquids on the disperse droplet's radius and formation frequency. The numerical simulation solves the transient Navier-Stokes equations in conjunction with the momentum jump condition across the interface between the growing disperse droplet and the co-flowing continuous liquid using a finite element method. In addition to tracking the evolving surface of the forming and growing droplet while being attached to the tip of the inner micro-tube, the solution predicts the conditions leading to the necking and eventual pinch off of the mono-disperse and poly-disperse droplets in the dripping regime.

The numerical approach used is validated by comparing its predictions of the disperse droplet radius with those reported by Hua et al. [22] for  $Q_c = 15 - 118$  ml/s (or  $Ca_c = 0.03 - 0.225$ ), spanning the dripping and jetting flow regimes. Values of other parameters used in the validation are:  $R_d = 80$   $\mu$ m,  $R_c = 300$   $\mu$ m,  $\rho_d = 1000$  kg/m<sup>3</sup>,  $\rho_c = 800$  kg/m<sup>3</sup>,  $\mu_d = 0.031$  Pa-s,  $\mu_c = 0.047$  Pa-s,  $\sigma_{d,c} = 98$  mN/m and,  $Q_d = 0.98$   $\mu$ l/s. The transition from the dripping to the jetting regime for forming disperse droplets is predicted to occur at  $Q_c = 78$  ml/s (or  $\bar{u}_c = 0.31$  m/s), the same as that reported by Hua et al. [22]. The calculated radii of the forming disperse droplets are in good agreement with those reported by Hua et al. [22].

The effects of various operation parameters and liquids properties on the radius and forming frequency of the disperse droplets in the dripping regime are parametrically investigated one at a time. This parametric analysis investigated the effects of the interfacial tension, velocities and viscosities of the two immiscible liquids and the diameters of the coaxial micro-tubes on the disperse droplet radius and forming frequency. The obtained numerical results are used to develop semi-empirical correlations of the dimensionless radius ( $r_d^*$ ) and corresponding formation frequency ( $f^*$ ) of the disperse droplets. The correlation for  $r_d^*$  is within +20% to -6%, while that for  $f^*$  is within +20% to -30% of the numerical calculations in the dripping regime (Eqs. 11 and 12).

The developed correlation for the dimensionless radius of the disperse droplets (Eq. (11)) in the dripping regime is within +10% to -14% of recently reported experimental measurements for the formation of water droplets in a co-axial continuous flow of salad oil in the dripping regime [17]. Such good agreement further confirms the soundness of the numerical method used and validates it

accurately for calculating the radius and the forming frequency of the disperse droplets in the dripping regime. The developed semi-empirical correlations are useful predictive tools for industrial applications and design of prototypes of micro-emulsions. Additional experimental results are needed to further validate the present correlations and extend the scope of the present work to the jetting regime.

#### ACKNOWLEDGMENTS

This research is funded by the University of New Mexico's Institute for Space and Nuclear Power Studies.

#### REFERENCES

- [1] Cygan, Z. T., Cabral, J. T., Beers, K. L. and Amis, E. J., Microfluidic platform for the generation of organic-phase microreactors, *Langmuir*, 2005, 21(8), 3629–3634.
- [2] Zeng, Y., Novak, R., Shuga, J., Smith, M. T. and Mathies, R. A., High-performance single cell genetic analysis using microfluidic emulsion generator arrays, *Anal. Chem.*, 2010, 82(8), 3183–3190.
- [3] Guan, G., Teshima, M., Sato, C., Son, S. M., Irfan, M. F., Kusakabe, K., Ikeda, N. and Lin, T.-J., Two-phase flow behavior in microtube reactors during biodiesel production from waste cooking oil, *AIChE Journal*, 2010, 56(5), 1383–1390.
- [4] Umbanhowar, P. B., Prasad, V. and Weitz, D. A., Monodisperse emulsion generation via drop break off in a coflowing stream, *Langmuir*, 2000, 16(2), 347–351.
- [5] Ulmeanu, M., Preparation and characterization of water in oil emulsion via drop break-off, *Colloids Surface A*, 2008, 316, 119–124.
- [6] Yuyama, H., Yamamoto, K., Shirafuji, K., Nagai, M., Ma, G.-H. and Omi, S., Preparation of polyurethaneurea (PUU) uniform spheres by SPG membrane emulsification technique, *J. Appl. Polym. Sci.*, 2000, 77(10), 2237–2245.
- [7] Yang, C.-H., Lin, Y.-S., Huang, K.-S., Huang, Y.-C., Wang, E.-C., Jhong, J.-Y. and Kuo, C.-Y., Microfluidic emulsification and sorting assisted preparation of monodisperse chitosan microparticles, *Lab on Chip*, 2009, 9(1), 145–150.
- [8] Jin, F., Gupta, N. R. and Stebe, K. J., The detachment of a viscous drop in a viscous solution in the presence of a soluble surfactant, *Phys. Fluids*, 2006, 18(2), paper no. 022103.
- [9] Zhang, X. and Basaran, O. A., An experimental study of dynamics of drop formation, *Phys. Fluids*, 1995, 7(6), 1184–1203.
- [10] Mason, T. G. and Bibette, J., Shear rupturing of droplets in complex fluids, *Langmuir*, 1997, 13(17), 4600–4613.
- [11] Vladisavljevic, G. T., Shimizu, M. and Nakashima, T., Preparation of monodisperse multiple emulsions at high production rates by multi-stage premix membrane emulsification, *J. Membrane Sci.*, 2004, 244, 97–106.
- [12] Anna, S. L., Bontoux, N. and Stone, H. A., Formation of dispersions using flow focusing in microchannels, *Appl. Phys. Letter*, 2003, 82(364), 364–366.
- [13] Cramer, C., Fischer, P. and Windhab, E. J., Drop formation in a co-flowing ambient fluid, *Chem. Eng. Sci.*, 2004, 59(15), 3045–3058.
- [14] Cubaud, T. and Mason, T. G., Capillary threads and viscous droplets in square microchannels, *Phys. Fluids*, 2008, 20(5), paper no. 053302.
- [15] Castro-Hernandez, E., Gundabala, V., Fernandez-Nieves, A. and Gordillo, J. M., Scaling the drop size in coflow experiments, *New J. Phys.*, 2009, 11(7), paper no. 075021.
- [16] Utada, A. S., Fernandez-Nieves, A., Stone, H. A. and Weitz, D. A., Dripping to jetting transitions in coflowing liquid streams, *Phys. Rev. Lett.*, 2007, 99(9), paper no. 094502.

- [17] Gu, Y., Kojima, H. and Miki, N., Theoretical analysis of 3D emulsion droplet generation by a device using coaxial glass tubes, *Sens. Actuators A: Phys.*, 2011, 169(2), 326–332.
- [18] Zagnoni, M., Anderson, J. and Cooper, J. M., Hysteresis in multiphase microfluidics at a T-junction, *Langmuir*, 2010, 26(12), 9416–9422.
- [19] Gupta, A., Murshed, S. M. S. and Kumar, R., Droplet formation and stability of flows in a microfluidic T-junction, *Appl. Phys. Letter*, 2009, 94(16), paper no. 164107.
- [20] Suryo, R. and Basaran, O. A., Tip streaming from a liquid drip forming from a tube in a co-flowing outer fluid, *Phys. Fluids*, 2006, 18(8), paper no. 082102.
- [21] Hong, Y. and Wang, F., Flow rate effect on droplet control in a co-flowing microfluidic device, *Microfluid Nanofluid*, 2007, 3(3), 341–346.
- [22] Hua, J., Zhang, B. and Lou, J., Numerical simulation of microdroplet formation in coflowing immiscible liquids, *AIChE Journal*, 2007, 53(10), 2534–2547.
- [23] Zhang, D. F. and Stone, H. A., Drop formation in viscous flows at a vertical capillary tube, *Phys. Fluids*, 1997, 9(8), 2234–2242
- [24] Zhang, X., Dynamics of drop formation in viscous flows, *Chem. Eng. Sci.*, 1999, 54(12), pp. 1759–1774.
- [25] Hirt, C. W. and Nichols, B. D., Volume of fluid (VOF) Method for the dynamics of free boundaries, *J. Computational Phys.*, 1981, 39, 201–225.
- [26] Brackbill, J. U., Kothe, D. B. and Zemach C., A continuum method for modeling surface tension, *J. Computational Phys.*, 1992, 100(2), 335–354.
- [27] Vempati, B., Panchagnula, M. V. and Neti, A. O. S., Numerical investigation of liquid-liquid coaxial flows, *J. Fluids Eng.*, 2007, 129(6), 713–719.
- [28] *Comsol CFD user's guide*, Comsol AB., Stockholm, 2010, 155–272, <http://www.comsol.com>.
- [29] Gada, V. H. and Sharma, A., On derivation and physical-interpretation of level set method based equations for two-phase flow simulations, *Numer. Heat Transfer B*, 2009, 56, 307–322.
- [30] Olsson, E., Kreiss, G. and Zahedi, S., A conservative level set method for two phase flow II, *J. Computational Phys*, 2007, 225(1), 785–807.

